J. Eur. Opt. Society-Rapid Publ. 2024, **20**, 42

https://doi.org/10.1051/jeos/2024040
Available online at: https://jeos.edpsciences.org

Journal of the European Optical Society-Rapid Publications

RESEARCH ARTICLE OPEN ACCESS

Transient dielectric function dynamics driven by coherent phonons in Bismuth crystal

Davide Boschetto[1,*] and Denis Morineau[2]

[1] Laboratoire d'Optique Appliquée, ENSTA Paris, CNRS, Ecole Polytechnique, Institut Polytechnique de Paris, 91761 Palaiseau, France
[2] Institut de Physique de Rennes, CNRS, Université de Rennes, UMR 6251, Rennes, France

Received 22 August 2024 / Accepted 10 October 2024

Abstract. In this study, we investigate the ultrafast transient dynamics of the dielectric function in bismuth crystal, excited by femtosecond laser pulses and modulated by coherent phonons. The primary aim is to understand the influence of the coherent A_{1g} phonon mode on the dielectric function and to characterize the nature of the quasi-steady state that persists for tens of picoseconds after the coherent oscillations vanish. Our findings reveal that the dielectric function undergoes damped oscillations corresponding to the A_{1g} phonon mode, with the real and imaginary parts of the dielectric function oscillating out of phase but sharing the same frequency and lifetime as the oscillatory component. Once the oscillations vanish, the system reaches a quasi-steady state around 20 ps after excitation. In this state, the dielectric function deviates significantly from the values expected for the liquid phase, indicating that no phase transition occurs, even though the calculated lattice temperature exceeds the melting point of bismuth. To probe the nature of this quasi-steady state, we compare the transient dielectric function to equilibrium ellipsometry measurements taken at various temperatures, ranging from room temperature to temperatures approaching the melting point. This comparison allows us to estimate the real and imaginary parts of the dielectric function as a function of temperature, particularly in a warmed state, where the crystal temperature is elevated but still below the melting threshold. The comparison reveals a clear discrepancy between the dielectric function values in the quasi-steady state and those measured in a thermally equilibrated warmed state. This suggests that the quasi-steady state cannot be solely attributed to crystal heating. Instead, we propose that the persistence of the quasi-steady state is because electron-hole recombination has not fully occurred within the measured time range.

Keywords: Ultrafast dynamics, Femtosecond pump-probe spectroscopy, Transient dielectric function, Ellipsometry, Bismuth.

1 Introduction

Femtosecond laser-solid interactions have uncovered novel non-equilibrium transient states of matter with unique properties [1]. A key characteristic of these states is the rapid increase in electron energy during the laser pulse, while the lattice remains comparatively cool until the electrons transfer their energy to the lattice [2]. Probing these transient states with sub-picosecond time resolution provides a powerful tool for observing the transition of excited electronic and atomic subsystems to equilibrium, a process that dictates the fundamental electronic, magnetic, and optical properties of materials [3]. Understanding these processes is crucial, as they govern various phenomena in nature, from photocatalysis to charge transport in nanojunctions, and hold the potential to reveal new transient phases, metastable states, and chemical reaction pathways [4].

Despite the well-characterized ground state properties of many materials, their excited states remain largely unexplored. Gaining a comprehensive understanding of how physical properties change in the excited state is crucial not only for advancing fundamental knowledge but also for expanding the range of potential applications. Pump-probe experiments have become a widely used technique for investigating these excited states across a diverse range of materials, from inorganic compounds [5] to organic systems [6]. This technique has also been instrumental in tracking coherent atomic oscillations within crystal

* Corresponding author: davide.boschetto@ensta.fr

structures in semimetals [7], semiconductors [8], and superconductors [9].

However, most experimental studies report only transient reflectivity changes, which offer limited insights into the fast processes occurring in these photoinduced states. Several parameters, including electron and phonon densities, temperatures, band structure, and electron-phonon coupling, undergo significant changes in the excited state. Since reflectivity is a complex function of these parameters, it cannot fully elucidate the interaction processes involved during the relaxation dynamics. Thus, reflectivity measurements alone provide an incomplete picture of the photo excited state. A more thorough analysis can be achieved by examining the time-dependent changes in the real and imaginary components of the dielectric function, which directly reflect modifications in the band structure.

Two primary techniques have been developed to recover the dielectric function: using a single white light pulse [10] or employing two simultaneous pulses at different angles [11]. Both methods have been successfully applied to optical phonon studies [10, 12]. The single white light pulse method offers broader spectral information but suffers from a reduced signal-to-noise ratio. In contrast, the double-probe setup, though limited to measuring one wavelength at a time, provides high sensitivity.

Bismuth has emerged as a prototype system for time-resolved studies due to its simple crystal structure and intriguing properties, such as the small overlap between conduction and valence bands at a single point in the Brillouin zone, resulting in low carrier density and a long electron mean free path. Previous studies have employed pump-probe techniques to characterize the time-dependent reflectivity of bismuth excited by femtosecond laser pulses [12], while optical pump-hard X-ray probe methods have revealed the structural dynamics with the necessary spatial resolution [13]. Experiments using soft X-rays have also been reported [14].

Recently, the transient behavior of bismuths dielectric function was investigated using a non-degenerate white light probe pulse [15], with a pump wavelength centered at 800 nm (1.55 eV). However, this non-degenerate configuration restricts our understanding of energy states significantly higher than those excited by the pump, as the white light probe primarily covers energy levels well beyond the pump energy (1.55 eV). On the other hand, a degenerate double-probe experiment on photoexcited bismuth reported only the steady-state dielectric function [12].

In this study, we focus on the dynamics of the real and imaginary parts of the dielectric function of photoexcited bismuth on an ultrafast time scale, modulated by coherent phonon displacement. Our observations span from the very early stages of femtosecond excitation to several tens of picoseconds. Additionally, we perform ellipsometry experiments on the same sample under equilibrium conditions at varying temperatures to extract the real and imaginary parts of the dielectric function as a function of crystal temperature. Comparing the values obtained from these two configurations allows us to gain further insights into the transient state of the photoexcited bismuth crystal.

2 Experimental configurations and data treatment

For this study, we conducted two types of experiments: ultrafast pump-double-probe spectroscopy to investigate the transient dynamics of photoexcited bismuth crystals, and equilibrium ellipsometry measurements as a function of temperature, with the aim of extracting the real and imaginary components of bismuths dielectric function at various sample temperatures.

2.1 Ultrafast pump-double-probe spectroscopy

The ultrafast pump-double-probe spectroscopy experiments, whose setup is shown in Figure 1, were conducted using a mode-locked Ti:Sapphire laser system custom-designed and constructed in our laboratory, which is not commercially available. This laser system provided pulses of approximately 50 fs duration, with a wavelength centered at 800 nm (1.55 eV), and an energy of 1 mJ per pulse at a repetition rate of 1 kHz.

The laser pulse was split into three pulses: one was used as a pump and the other two as probes. The wavelengths of the three pulses were identical, so the experiments were conducted in a degenerate pump/double-probe configuration. All beams had Gaussian spatial profiles, measured by a Charge Coupled Device (CCD-camera, model Ganz 25C) with a 4.5×-zoom objective. The pump pulse focal spot on the sample surface was 120 μm, while the two probes were focused to 20 μm, ensuring homogeneous probing of the excited surface. To ensure that the superposition of the three pulses on the sample surface was unaffected by the delay line's motion, we used the CCD camera to monitor the pulse overlap across the entire measured time range. No changes in the pump and probe superposition were detected. The setup also confirmed that moving the delay line did not cause any displacement of the focal spots or changes in the spot sizes of the three beams on the sample plane. The pump and probe fluences were kept constant at 6.9 mJ/cm^2 and 10 μJ/cm^2, respectively.

The pump pulse passed through a commercial optical chopper (model 300CD from Scitec Instruments) that reduced the pump pulse repetition rate to 0.5 kHz (half of the laser repetition rate) by selecting one pulse out of two, while the probe pulses maintained the laser's original repetition rate of 1 kHz. In order to ensure synchronization between the optical chopper and the pump pulse, we used a commercial optical chopper synchronizer equipped with a phase-locked loop (model 300Synch from Scitec Instruments). This approach enables the detection of subtle changes in reflectivity, as demonstrated in several previous studies [2, 3, 5, 6, 12]. The pump beam was p-polarized, while the two probe beams, arriving at different angles on the sample surface, were s-polarized. After reflection, the pump pulse is stopped by a beam blocker. Since the pump and probe pulses have orthogonal polarizations, two analyzers were placed in front of each photodiode. These analyzers are configured to filter out the pump pulse polarization, significantly reducing the number of pump photons reaching

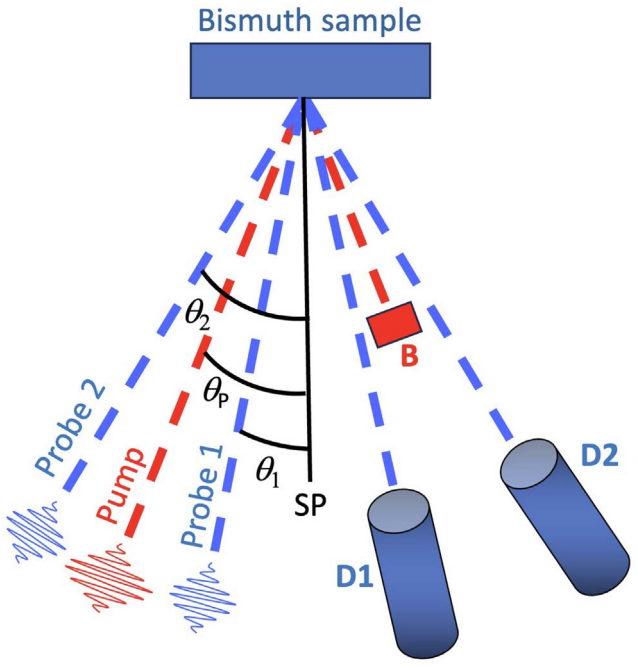

Fig. 1. Experimental configuration for ultrafast pump- double-probe spectroscopy. The two probe pulses arrive at two different angles $\theta_1 = 19.5°$ and $\theta_2 = 34.5°$, respectively. The pump pulse arrives in-between the two probe pulses, at an angle $\theta_P = (\theta_2 + \theta_1)/2$. In the figure, the vertical black line labelled SP is the surface's perpendicular, from which the angles are measured. The two probe pulses are measured by the two photodiodes D1 and D2, respectively, while the reflected pump pulse is blocked by the beam blocker B.

the detector and ensuring that primarily the reflected probe pulses are measured.

The angles for the two probe pulses were chosen as $\theta_1 = 19.5°$ and $\theta_2 = 34.5°$ (measured with respect to the normal incident axis, as shown in Fig. 1), while the pump pulse was directed at the midpoint between these two angles, *i.e.*, $\theta_P = (\theta_2 + \theta_1)/2$. These angles were selected to minimize uncertainty in the dielectric function after the numerical inversion of Fresnel formulas and to prevent any degradation in temporal resolution due to geometrical factors. The temporal resolution of this setup, measured through cross-correlation on a Beta Barium Borate (BBO) crystal, was approximately 70 fs.

The two probe pulses were temporally synchronized, and a delay line on the pump pulse was used to control the arrival delay of the pump with respect to the probe pulses. The probe pulses were detected by two photodiodes, each one connected to a lock-in amplifier (Stanford Research Systems, model SR830), which was synchronized with the pump pulse repetition rate (i.e. at 0.5 kHz). By using the 0.5 kHz reference, the lock-in amplifier isolates the signal corresponding to the pump-induced changes in the probe pulses. It accomplishes this by multiplying the incoming signal with a reference signal at 0.5 kHz and then applying a low-pass filter. This process extracts the component at the reference frequency (0.5 kHz), effectively filtering out noise and scattering contributions at other frequencies. This setup enabled the measurement of relative changes in reflectivity with a very high signal-to-noise ratio, achieving measurement accuracy of approximately $\Delta R/R \approx 10^{-5}$ [2, 3, 5, 6, 12].

The sample used was a (1 1 1)-oriented single crystal of bismuth, aligned with the trigonal cell representation. As bismuth is a uniaxial crystal, the s-polarized probes were sensitive to changes in the plane orthogonal to the optical axis. Therefore, the measured dielectric function corresponds to the ordinary dielectric function.

2.2 Retrieving the dielectric function

For an s-polarized beam incident on the samples surface at an angle θ_i with respect to the surface normal, the reflectivity can be expressed using the Fresnel equation as [16]:

$$R_i = \left| \frac{\cos\theta_i - \sqrt{\epsilon_{\mathrm{Re}} + i\epsilon_{\mathrm{Im}} - \sin^2\theta_i}}{\cos\theta_i + \sqrt{\epsilon_{\mathrm{Re}} + i\epsilon_{\mathrm{Im}} - \sin^2\theta_i}} \right|^2, \quad (1)$$

where ϵ_{Re} and ϵ_{Im} represent the real and imaginary parts of the dielectric function, respectively. At fixed values of ϵ_{Re} and ϵ_{Im}, the reflectivity becomes a function of the incident angle θ_i, *i.e.*:

$$R_i = f(\theta_i; \epsilon_{\mathrm{Re}}, \epsilon_{\mathrm{Im}}). \quad (2)$$

When using two probe pulses arriving at different angles, θ_1 and θ_2, the system of equations becomes:

$$R_1 = f(\theta_1; \epsilon_{\mathrm{Re}}, \epsilon_{\mathrm{Im}}) \quad \text{and} \quad R_2 = f(\theta_2; \epsilon_{\mathrm{Re}}, \epsilon_{\mathrm{Im}}). \quad (3)$$

Given that the values of R_1, R_2, θ_1, and θ_2 are known experimentally, this system allows us to calculate the two unknowns, ϵ_{Re} and ϵ_{Im}.

However, the system of equations in (3) is nonlinear and cannot be solved directly. To address this, we apply the Newton-Raphson Method (NRM), as described in [17]. This algorithm is performed at every pump-probe time delay in order to recover the transient values of both the real and imaginary parts of the dielectric function.

2.3 Equilibrium ellipsometry setup

The equilibrium ellipsometry measurements were conducted at an incidence angle of 70° using a Horiba (UVISEL) spectroscopic ellipsometer, covering the optical range from 280 to 2000 nm. The sample temperature was controlled using a Linkam THMS600 heating stage.

Ellipsometry was performed at five different sample temperatures: 21 °C, 50 °C, 100 °C, 150 °C, and 200 °C. Data acquisition for each temperature was carried out after thermal stabilization of the sample. The real and imaginary parts of the dielectric function were determined from the ellipsometric angles, assuming a planar semi-infinite model.

3 Results and discussion

Figure 2 shows the transient change in reflectivity measured at two different angles, $\theta_1 = 19.5°$ and $\theta_2 = 34.5°$, with a

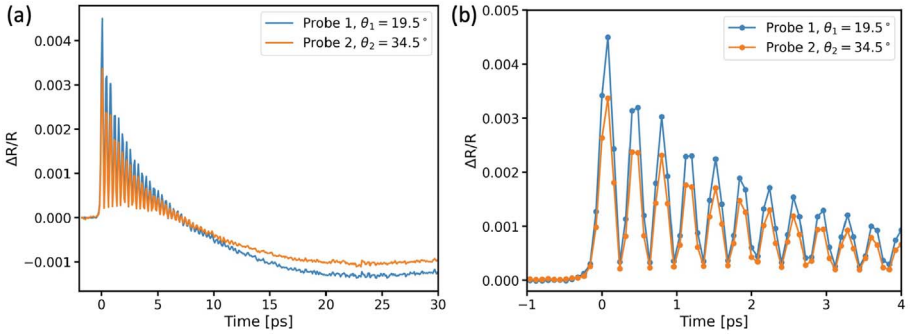

Fig. 2. Experimental reflectivities of the two probe pulses, arriving at the angle $\theta_1 = 19.5°$ (blue line) and $\theta_2 = 34.5°$ (orange line), respectively. (a) Full measured time range. (b) Zoom-in on the first 4 ps, with data points marked by circles for better visibility.

pump fluence of 6.9 mJ/cm^2. The transient behavior is characterized by an initial increase in reflectivity, followed by relaxation superimposed on a damped oscillation. The behavior is similar at both angles, consistent with previously reported results [12, 18, 19]. However, the two signals differ quantitatively. Using the approach described in Section 2.2, we can retrieve the transient changes in the real and imaginary parts of the dielectric function.

Figure 3 presents the dynamics of the real and imaginary parts of the dielectric function, recovered from the data shown in Figure 2. The unperturbed dielectric function at $t < 0$ aligns well with previously reported literature values [20, 21].

The temporal evolution of both the real and imaginary parts of the dielectric function exhibits features akin to those observed in reflectivity measurements (Fig. 2). Following the initial fast excitation, damped oscillations are observed, with a frequency corresponding to the A_{1g} phonon mode in Bi, approximately 2.8 THz. These oscillations diminish within several picoseconds, leading to a transition to a quasi-stationary value, forming a plateau around 20 ps post-excitation. This plateau is a quasi-steady state, which persists for approximately 4 ns before the system returns to its initial equilibrium state.

Immediately after excitation, there is a noticeable increase in the imaginary part and a decrease in the real part, with both components oscillating out of phase but sharing the same frequency and lifetime. Notably, the oscillation amplitude of the imaginary part is larger than that of the real part. From the values at the first oscillation peak, we extrapolate a relative increase in absorption of approximately 30%, corresponding to a decrease in the penetration depth of about 25% from the equilibrium value of roughly 20 nm. This is consistent with the higher electron density excited by the pump pulse, which leads to an increase in absorption.

The oscillatory behavior of the real and imaginary parts of the dielectric function is consistent with the notion that when a coherent phonon mode is established within the crystal, the entire band structure is modified quasi-instantaneously by this mode, thereby altering the optical properties in tandem with the changes in the band structure. This observation is also in agreement with femtosecond ARPES measurements [22].

To extract more quantitative information about this dynamic, we performed a fit using the following equation:

$$S(t) = A \cdot \exp\left(-\frac{t}{\tau_{ph}}\right) \cdot \cos\left[2\pi\omega(t) \cdot t + \phi\right] + B \cdot \exp\left(-\frac{t}{\tau}\right) + C, \quad (4)$$

where $S(t)$ is the signal, either ϵ_{Re} or ϵ_{Im}, A is the amplitude of the oscillatory component, τ_{ph} is the coherent phonon lifetime, $\omega(t)$ is the time-dependent coherent phonon frequency, ϕ is the phase, B is the amplitude of the baseline of the oscillation, τ is the relaxation time of the baseline, and C is the plateau value.

For the frequency $\omega(t)$, we used a time-dependent form to account for the changes in frequency over time. Previous studies have reported a fluence-dependent initial red shift of the phonon frequency [19], followed by a recovery toward the equilibrium Raman value. Based on our experimental results, the best fitting function for the frequency is:

$$\omega(t) = \omega_0 - \Delta\omega \cdot \exp(-t/\tau_0) \quad (5)$$

where ω_0 is the equilibrium Raman value (for the A_{1g} mode of bismuth, $\omega_0 = 2.92$ THz [12]), $\Delta\omega$ is the initial red-shift of the frequency, and $1/\tau_0$ is the rate at which the frequency returns to the equilibrium Raman value.

The best fits for both the real and imaginary parts of the dielectric function are shown by the grey dashed lines in Figure 3. The relevant fitting parameters include the phonon frequency, the phonon damping time, and the decay time of the baseline. For both the real and imaginary parts of the dielectric function, the best-fitting parameters were as follows. For the phonon parameters, the frequency redshift was found to be $\Delta\omega = 0.22$ THz, and the recovery time constant was $\tau_0 = 10$ ps. The phonon damping time was $\tau_{\mathrm{ph}} = 3.6$ ps. These values are consistent with previous studies [18, 19]. For the exponential decay of the baseline, the fitting yielded $\tau = 6.66$ ps.

Remarkably, when analyzing the imaginary part of the dielectric function, the first oscillation (*i.e.*, the maximum of the signal) strongly deviates from the fitting curve. This deviation could be attributed to the influence of the increased population of photoexcited carriers on the

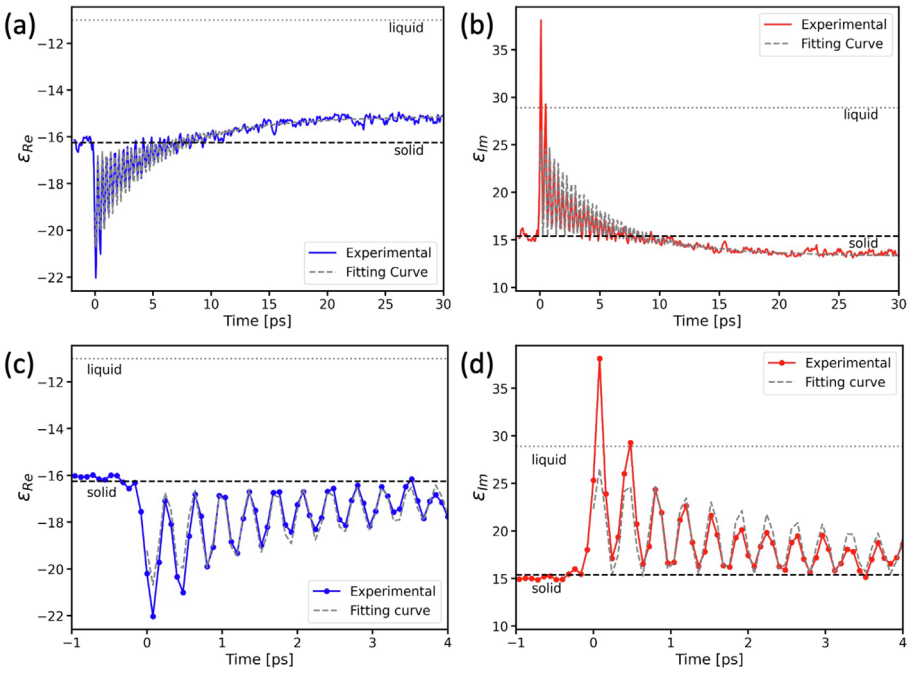

Fig. 3. Real (ϵ_{Re}, in blue) and imaginary (ϵ_{Im}, in red) part of the dielectric function versus pump-probe time delay. The values of ϵ_{Re} and ϵ_{Im} for the solid and liquid phase are shown by horizontal dashed lines. The fitting curves, explained in the main text, are shown as grey dashed lines. (a) ϵ_{Re} in the full measured time range. (b) ϵ_{Im} in the full measured time range. (c) Zoom-in of ϵ_{Re} on the first 4 ps, with data points marked by circles for better visibility. (d) Zoom-in of ϵ_{Im} on the first 4 ps, with data points marked by circles for better visibility.

imaginary part of the dielectric function, potentially explaining the additional rise superimposed on the oscillations. We also observe a slight deviation in the behavior of the baseline at the plateau. This could be related to more complex interactions between the different degrees of freedom in the crystal, such as the thermal exchange between the electron and phonon subsystems [18], which are not accounted for in our simplified fitting model.

We now focus on the values of both the real and imaginary parts of the dielectric function at the plateau, in order to better understand the nature of this quasi-steady state. Interestingly, at the plateau, the real part of the dielectric function is higher ($\varepsilon^{\mathrm{tr}}_{\mathrm{Re}} = -15.2 \pm 0.10$) than in the solid state ($\varepsilon^{\mathrm{s}}_{\mathrm{Re}} = -16.25$), while the imaginary part is lower ($\epsilon^{\mathrm{tr}}_{\mathrm{Im}} = 13.6 \pm 0.2$) compared to the solid state ($\epsilon^{\mathrm{s}}_{\mathrm{Im}} = 15.4$). Moreover, the observed changes in both the real and imaginary parts move in the opposite direction to those expected for a transition to the liquid phase, where $\varepsilon^{\mathrm{liq}}_{\mathrm{Re}} = -11$ and $\varepsilon^{\mathrm{liq}}_{\mathrm{Im}} = 28.9$ [23].

These results indicate that no phase transition to the liquid state occurs. At first glance, this may seem unexpected, as the calculated maximum lattice temperature T_L for a pump fluence $F = 6.9\ \mathrm{mJ/cm^2}$ is around 1300 K, based on energy conservation. This temperature is significantly higher than the melting point of approximately 544 K [20, 21]. However, recent studies [24] have shown that the high electron temperature gradient facilitates the transport of electrons out of the heated zone. Consequently, thermalization occurs over a much larger volume than the initially excited region, resulting in a significantly lower increase in lattice temperature. The increase in lattice temperature can be estimated by analyzing the relative change in reflectivity at the plateau. Previous measurements of reflectivity changes due to lattice heating [7] yielded $\frac{\mathrm{d}(\Delta R/R)}{\mathrm{d}T} \approx -8 \times 10^{-5}\ \mathrm{K}^{-1}$. Using this value and considering the relative change in reflectivity at the plateau, we estimate the rise in lattice temperature after 20 ps to be approximately 12 K, which is consistent with the absence of a solid-to-liquid phase transition. This conclusion is further supported by a double-pump single-probe experiment conducted under the same experimental conditions [12], with the second pump pulse arriving around 25 ps after the first one, demonstrating that the second pump pulse induces a similar behavior. If a transition to the liquid phase had occurred, the phonon parameters would have been different due to the distinct bonding state in the liquid phase compared to the solid state.

We might therefore be tempted to attribute the plateau observed in the real and imaginary parts of the dielectric function to a merely warmed state. Instead, in previous work [12], it was already suggested that this transient state is not merely a warm state, though no experimental evidence was provided. To test this hypothesis, we compared the values of the dielectric function at the quasi-steady state to those obtained at thermal equilibrium for increasing crystal temperatures. For this purpose, we conducted ellipsometry measurements at equilibrium [25] as a function of the sample temperature, using the same sample as in the transient dielectric function experiments. If the plateau observed after 20 ps in Figure 3 corresponded to a merely

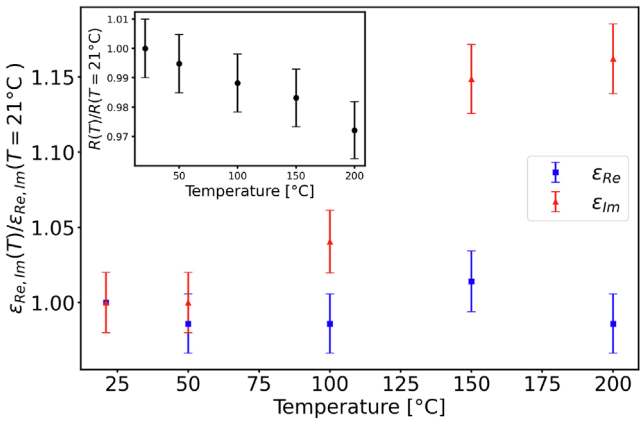

Fig. 4. Relative change of ϵ_{Re} (blue) and ϵ_{Im} (red) as function of the crystal temperature, by ellipsometry measurement at equilibrium. The inset shows the relative change of the reflectivity in the same range of temperatures.

warmed state, both the real and imaginary parts of the dielectric function would match the values of heated bismuth, as measured through equilibrium ellipsometry.

Figure 4 shows the relative changes in the real and imaginary parts of the dielectric function at 800 nm as a function of crystal temperature under equilibrium conditions. These measurements were performed over a temperature range from room temperature to 200 °C, which is below the melting point of 271 °C. From Figure 4, we observe that as the crystal heats, the imaginary part increases, while the real part remains constant within the error bars.

However, in the transient measurements (Fig. 3), at the plateau, the real and imaginary parts of the dielectric function do not follow this trend; instead, we observe the opposite: the imaginary part decreases, and the real part increases. This discrepancy indicates that the dielectric function at the quasi-steady state is not simply due to crystal heating. If the system were merely heated, the values of the dielectric function at the plateau should resemble the equilibrium temperature-dependent behavior seen in Figure 4. Since they do not, we can conclude that the plateau in the dielectric function corresponds to a more complex non-equilibrium state, rather than a merely warmed state. This suggests that other processes are responsible for the observed behavior.

The occurrence of a phase transition from a semimetallic to a semiconducting state in bismuth at a pressure of approximately 2.5 GPa has also been reported [26]. However, in this phase, the crystal structure does not support the existence of the A_{1g} phonon mode, as has been experimentally demonstrated. In contrast, at the plateau, we can still excite this coherent phonon, as shown in [12]. Therefore, the hypothesis that the transient plateau corresponds to a photoinduced phase transition can also be ruled out.

One possible explanation for the differing behavior of the transient dielectric function at the plateau (Fig. 3) compared to the equilibrium dielectric function versus crystal temperature (Fig. 4) is that electron-hole recombination has not yet occurred after 20 ps. Consequently, the surface of the bismuth crystal remains in a heated excited state. Equilibrium measurements [27] show an electron-hole recombination time of a few nanoseconds at temperatures around 10 K and a few picoseconds at room temperature. However, the recombination rate can be significantly altered in femtosecond pump-probe experiments. Indeed, the energy relaxation channels in the photoexcited state may differ from those at equilibrium, especially under high-density photoexcitation, as has been demonstrated in semiconductor quantum dots [3].

A deeper investigation into the modifications in the band structure of photoexcited bismuth is warranted to further unveil the nature of this quasi-steady state. This could include recovering the transient dielectric function dynamics over a broader spectral range.

4 Conclusions

In conclusion, the temporal evolution of the complex dielectric function at 1.55 eV in the transient state of femtosecond laser-excited bismuth has been successfully recovered using dual-angle reflectivity measurements with 70 fs resolution. These results reveal how coherent phonons influence the real and imaginary parts of the dielectric function, a phenomenon that can be attributed to transient changes in the band structure. The comparison between the transient behavior of the dielectric function and ellipsometry measurements conducted at equilibrium across varying temperatures indicates that, at the plateau, the crystal is not merely in a heated state. Indeed, the values of the real and imaginary parts of the dielectric function differ both qualitatively and quantitatively from those of the heated crystal at equilibrium, suggesting that other processes are responsible for this quasi steady state. We attribute this quasi-steady state to delayed electron-hole recombination, meaning that electrons and holes have not fully recombined even after tens of picoseconds. This contrasts sharply with the much faster recombination times typically observed under equilibrium conditions. This discrepancy suggests that the energy relaxation channels in the photoexcited state may differ significantly from those at equilibrium. Further, time-resolved studies, including time-resolved diffraction [28, 29], time-resolved ARPES [22], and the recovery of the dielectric function of bismuth across a broader spectral range around the pump photon energy, will be essential for gaining a deeper understanding of the photoinduced changes in the band structure.

Acknowledgments

The authors acknowledge Andrei Rode and Eugene Gamaly from the Australian National University for their kind help in the experimental set-up and fruitful discussions on the results. The support of Programme International De Cooperation Scientifique (PICS, France) as well as the European contract FLASH (number MRTN-CT-2003-503641) is gratefully acknowledged.

Funding

This research received no external funding.

Conflicts of interest

The authors declare no conflicts of interest.

Data availability statement

Data obtained in this work are not publicly available but may be obtained from the authors upon reasonable request.

Author contribution statement

Conceptualization, D.B.; methodology, D.B.; Measurement of transient reflectivity, D.B.; Theoretical calculations and simulations, D.B.; Measurement of equilibrium ellipsometry, D.M.; Original draft preparation, D.B.; Review and editing of the original draft, D.B. and D.M.

References

1 Budden M, Gebert T, Buzzi M, Jotzu G, Wang E, Matsuyama T, Meier G, Laplace Y, Pontiroli D, Ricco M, Schlawin F, Jaksch D, Cavalleri A, Evidence for metastable photo-induced superconductivity in $K_3C_{60,}$ *Nat. Phys.* **17**(5), 611–618 (2021).

2 Lejman M, Weis M, Nilforoushan N, Faure J, Ta Phuoc V, Cario L, Boschetto D, Ultrafast photoinduced conductivity reduction by bonding orbital control in an incommensurate crystal, *Phys. Rev. B* **108**, 134306 (2023).

3 Khalili A, Weis M, Mizrahi SG, Chu A, Dang TH, Abadie C, Gréboval C, Dabard C, Prado Y, Xu XZ, Péronne E, Livache C, Ithurria S, Patriarche G, Ramade J, Vincent G, Boschetto D, Lhuillier E, Guided-mode resonator coupled with nanocrystal intraband absorption, *ACS Photon.* **9**, 985–993 (2022).

4 Maiuri M, Garavelli M, Cerullo G, Ultrafast spectroscopy: State of the art and open challenges*, J. Am. Chem. Soc.* **142** (1), 3–15 (2020).

5 Mansart B, Boschetto D, Sauvage S, Rousse A, Marsi M, Mott transition in Cr-doped V_2O_3 studied by ultrafast reflectivity: Electron correlation effects on the transient response, *Europhys. Lett.* **92**, 37007 (2010).

6 Servol M, Moisan N, Collet E, Cailleau H, Kaszub W, Toupet L, Boschetto D, Ishikawa T, Moréac A, Koshihara S, Maesato M, Uruichi M, Shao X, Nakano Y, Yamochi H, Saito G, Lorenc M, Local response to light excitation in the charge-ordered phase of $(EDO{-}TTF)_2SbF_{6,}$ *Phys. Rev. B* **92**, 024304 (2015).

7 Wu AQ, Xu X, Coupling of ultrafast laser energy to coherent phonons in bismuth, *Appl.Phys. Lett.* **90**, 251111 (2007)

8 Roeser CAD, Kandyla M, Mendioroz A, Mazur E, Optical control of coherent lattice vibrations in tellurium, *Phys. Rev. B* **70**, 212302 (2004).

9 Ramos-Alvarez A, Fleischmann N, Vidas L, Fernandez-Rodriguez A, Palau A, Wall S, Probing the lattice anharmonicity of superconducting $YBa_2Cu_3O_{7-\delta}$ via phonon harmonics, *Phys. Rev. B* **100**, 184302 (2019).

10 Richter S, Rebarz M, Herrfurth O, Espinoza S, Schmidt-Grund R, Andreasson J, Broadband femtosecond spectroscopic ellipsometry, *Rev. Scientific Instrum.* **92**, 033104 (2021).

11 Roeser CAD, Kim AM-T, Callan JP, Huang L, Glezer EN, Siegal Y, Mazur E, Femtosecond time-resolved dielectric function measurements by dual-angle reflectometry, *Rev. Scientific Instrum.* **74**, 3413–3422 (2003).

12 Boschetto D, Garl T, Rousse A, Ultrafast dielectric function dynamics in bismuth, *J. Modern Opt.* **57** (11), 953–958 (2010).

13 Fritz DM, Reis DA, Adams B, Akre RA, Arthur J, Blome C, Bucksbaum PH, Cavalieri AL, Engemann S, Fahy S, Falcone RW, Fuoss PH, Gaffney KJ, George MJ, Hajdu J, Hertlein MP, Hillyard PB, von Hoegen MH, Kammler M, Kaspar J, Kienberger R, Krejcik P, Lee SH, Lindenberg AM, McFarland B, Meyer D, Montagne T, Murray ED, Nelson AJ, Nicoul M, Pahl R, Rudati J, Schlarb H, Siddons DP, Sokolowski-Tinten K, Tschentscher T, von der Linde D, Hastings JB, Ultrafast bond softening in bismuth: Mapping a solid's interatomic potential with X-rays, *Science* **315** (5812), 633–636 (2007).

14 Papalazarou E, Boschetto D, Gautier J, Garl T, Valentin C, Rey G, Zeitoun P, Rousse A, Balcou P, Marsi M, Probing coherently excited optical phonons by extreme ultraviolet radiation with femtosecond time resolution, *Appl. Phys. Lett.* **93**, 041114 (2008).

15 Thiemann F, Sciaini G, Kassen A, Lott TS, Horn-von Hoegen M, Disentangling the electronic and lattice contributions to the dielectric response of photoexcited bismuth, *Phys. Rev. B* **109**, L041105 (2024).

16 Born M, Wolf E. *Principles of optics* (Pergamon Press, Oxford, UK, 1980).

17 Press WH, Teukolsky SA, Vetterling WT, Flannery BP. *Numerical Recipes in Fortran 77*, 2nd ed. (Cambridge University Press, Cambridge, UK, 1992).

18 Boschetto D, Gamaly EG, Rode AV, Luther-Davies B, Glijer D, Garl T, Albert O, Rousse A, Etchepare J, Small atomic displacements recorded in bismuth by the optical reflectivity of femtosecond laser-pulse excitations, *Phys. Rev. Lett.* **100**, 027404 (2008).

19 Garl T, Gamaly EG, Boschetto D, Rode AV, Luther-Davies B, Rousse A, Birth and decay of coherent optical phonons in femtosecond-laser-excited bismuth, *Phys. Rev. B* **78**, 134302 (2008).

20 Madelung O, Schulz M, Weiss H (eds.) *Numerical Data and Functional Relationships in Science and Technology*, vol. 17 of *Landolt-Börnstein, New Series, Group III* (Springer-Verlag, Berlin, 1983).

21 Madelung O, Rössler U, Schulz M. *Numerical data and functional relationships in science and technology, vol. 41C of Landolt-Bornstein, New Series, Group III* (Springer-Verlag, Berlin, 2006)

22 Faure J, Mauchain J, Papalazarou E, Marsi M, Boschetto D, Timrov I, Vast N, Ohtsubo Y, Arnaud B, Perfetti L, Direct observation of electron thermalization and electron-phonon coupling in photoexcited bismuth, *Phys. Rev. B* **88**, 075120 (2013).

23 Comins NR The optical properties of liquid metals, *Phil. Mag. A J. Theo. Exp. Appl. Phys.* **25** (4), 817–831 (1972).

24 Jnawali G, Boschetto D, Malard LM, Heinz TF, Sciaini G, Thiemann F, Payer T, Kremeyer L, Meyer zu Heringdorf F.-J., Horn-von Hoegen M, Hot carrier transport limits the displacive excitation of coherent phonons in bismuth, *Appl. Phys. Lett.* **119**, 091601 (2021).

25 Spenato D, Dubreuil M, Morineau D, Giamarchi P, Dekadkevi D, Jay J-P, Fessant A, Rivet S, Grand YL, Ta/NiO subwavelength bilayer for wide gamut, strong interference structural color, *J. Phys. Commun.* **6**, 035002 (2022).

26 Kasami M, Mishina T, Nakahara J, Femtosecond pump and probe spectroscopy in bi under high pressure, *Physica Status Solidi: B* **241**(14), 3113–3116 (2004).
27 Lopez AA, Electron-hole recombination in bismuth, *Phys. Rev.* **175**, 823–840 (1968).
28 Sciaini G, Harb M, Kruglik SG, Payer T, Hebeisen CT, Heringdorf F-JMZ, Yamaguchi M, Hoegen MH-V, Ernstorfer R, Miller RJD, Electronic acceleration of atomic motions and disordering in bismuth, *Nature* **458**(7234), 56–59 (2009).
29 Gonzalez Vallejo I, Gallé G, Arnaud B, Scott SA, Lagally MG, Boschetto D, Coulon P-E, Rizza G, Houdellier F, Le Bolloćh D, Faure J, Observation of large multiple scattering effects in ultrafast electron diffraction on monocrystalline silicon, *Phys. Rev. B* **97**, 054302 (2018).